Bioinspiration & Biomimetics

PAPER

Bioinspired buckling of scaled skins

RECEIVED
28 January 2021

REVISED
11 March 2021

ACCEPTED FOR PUBLICATION
30 April 2021

PUBLISHED
7 June 2021

Ali Shafiei[1], **J William Pro**[1] **and Francois Barthelat**[1,2,*]

[1] Department of Mechanical Engineering, McGill University, 817 Sherbrooke Street West, Montreal, QC H3A 2K6, Canada
[2] Department of Mechanical Engineering, University of Colorado, 427 UCB, 1111 Engineering Dr, Boulder, CO 80309, United States of America
[*] Author to whom any correspondence should be addressed.

E-mail: francois.barthelat@colorado.edu

Keywords: bioinspiration, discrete element method, segmented hard material, buckling, stability

Abstract

Natural flexural armors combine hard, discrete scales attached to soft tissues, providing unique combinations of surface hardness (for protection) and flexibility (for unimpeded motion). Scaled skins are now inspiring synthetic protective materials which offer attractive properties, but which still suffer from limited trade-offs between flexibility and protection. In particular, bending a scaled skin with the scales on the intrados side jams the scales and stiffen the system significantly, which is not desirable in systems like gloves where scales must cover the palm side. Nature appears to have solved this problem by creating scaled skins that can form wrinkles and folds, a very effective mechanism to accommodate large bending deformations and to maintain flexural compliance. This study is inspired from these observations: we explored how rigid scales on a soft membrane can buckle and fold in a controlled way. We examined the energetics of buckling and stability of different buckling modes using a combination of discrete element modeling and experiments. In particular, we demonstrate how scales can induce a stable mode II buckling, which is required for the formation of wrinkles and which could increase the overall flexural compliance and agility of bioinspired protective elements.

1. Introduction

The need for protection against predation and other threats in nature has led to high performance protective systems that evolved over millions of years. Among natural flexible armor, scaled skins are common in animals including fish, snakes, lizards, and armadillos. The main idea in scaled skins is to cover flexible tissues with hard plates of finite sizes [1–5]. The hard plates provide surface hardness and resistance to puncture and laceration [6–9], while also maintaining high flexural compliance due to the ability of discrete scales to move relative to one another. These systems have been inspiring synthetic scaled protective systems [1–5], where a central design challenge is to combine high puncture resistance with flexural compliance [2, 10–19]. In these systems the architecture and arrangement of the scales can be tuned to maximize combinations of compliance and protection [1–3, 10, 11, 15, 17, 20, 21]. However, a major challenge remains: it is difficult to achieve high compliance when hard scales are placed on the 'intrados' side of the skin (i.e. inside the curvature) because at large flexural deformations the scales come closer together, enter contact and can jam, causing significant stiffening in flexion [10, 11, 16, 22, 23]. This scenario is not observed in flexible skins made purely of soft tissues, for example in the skin on the palm of human hands. When the hand closes the skin undergoes flexural deformations combined with compression in the plan of the skin, because the skin is offset by ∼10 mm from the rotation axes of the joints. The skin can buckle and form wrinkles to accommodate deformations (figure 1(a), [24]), which maintains large compliance even when the hand is completely closed. In contrast, we recently covered the palm of Kevlar gloves with alumina scales following a stretch and release protocol [11]. This glove is impervious to lacerations and sharp punctures, but the wearer of the glove feels a sharp stiffening as they close their hands and as the ceramic scales jam together (figure 1(b)). In this glove the scales completely suppress the wrinkling and folding mechanisms which are so important for the overall compliance of skin (and also for the compliance of a scale-less protective glove). Is it possible to create scaled skins that can

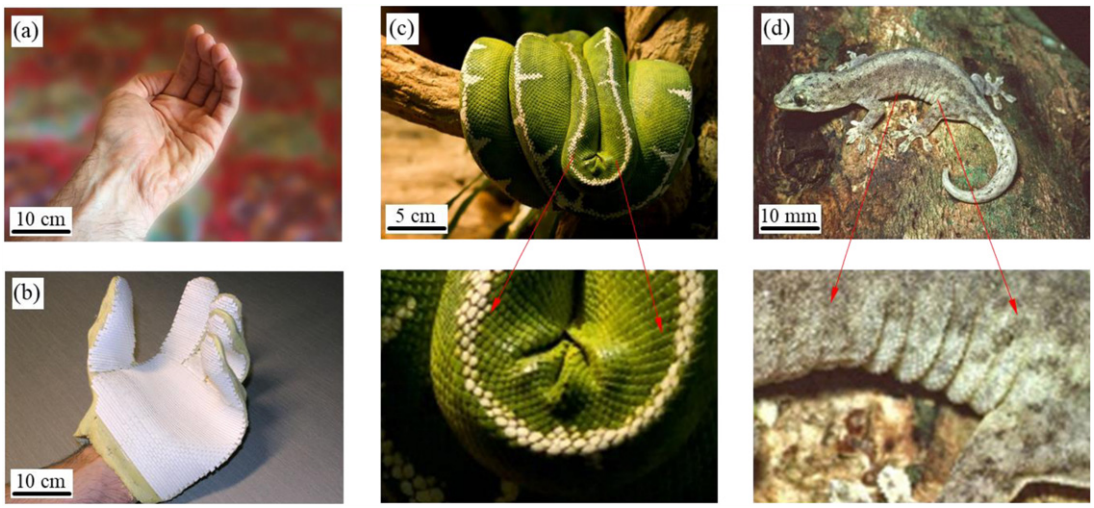

Figure 1. (a) Buckling/folding/flexure of skin at the palm of a hand allows for high compliance; (b) However hard ceramic scales at the palm of a Kevlar glove suppress these mechanisms: the scales jam and significant stiffening is felt when the hand is closed. Nature demonstrates that the buckling/folding of scaled skins is possible: (c) Emerald tree boa snake (*C. caninus*, reproduced with permission from [25]); (d) Christmas Island chained gecko (*L. listeri*, reproduced with permission from [26]).

buckle and form wrinkles? This design, which would be very attractive for regions of high deformation like the palm of a glove, does not exist in synthetic systems. Interestingly however, buckling and wrinkling of scaled skins do exist in nature. Figures 1(d) and (e) show examples of a snake and a lizard with sections of their bodies undergoing high flexural deformations. The intrados side of the scaled skin clearly forms wrinkles to accommodate for large deformations without resistance, preventing the scales from jamming together in these regions of high compression. Can we duplicate these buckling and folding mechanisms in synthetic scaled skins? The objective of this work is to investigate how hard scales on a flexible membrane affect the buckling energy landscape, and how in certain cases the stability of buckling modes can be manipulated.

To investigate these mechanisms we used the discrete element method (DEM), a computational efficient approach which was initially developed by Cundall' and Strack for granular materials [27] and which was more recently used to model deformation and fracture in staggered composites such as enamel, nacre, Bouligand-type structures, and fish-skin-like material [16, 28–32]. For this study we applied DEM to the buckling of scaled membranes, and after validation against experiments, we examined the effect of the architecture and the arrangement of the scales on buckling response and stability of different buckling modes.

2. DEM model setup and validation

The objective of this work is to capture the mechanics of deformation of bioinspired scaled membranes using 2D models and experiments, focusing on the interplay between membrane deformation and scale-scale interactions. These mechanisms involve contact mechanics and large deformations, making them computationally expensive to capture with traditional modeling approach such as finite elements. As an alternative we used the DEM, which is much more computationally efficient for this type of problem [27]. The main assumption of this modeling approach is that the scales are rigid in comparison to the membrane on which they are attached. Each scale was therefore modeled as a discrete element with its own given geometry and three degrees of freedom (two translations and one rotation). The scales were perfectly bonded on the surface of a 2D flexible membrane which was modeled with a series of nonlinear beam elements [16]. While the scales were assumed to be rigid compared to the membrane, their elastic deformation was taken into account in the case of direct contact with other scales (more details are provided below). The membrane was modeled as a linear elastic material (modulus E) with second moment of area I (which included the effect of membrane thickness) using nonlinear co-rotational Euler–Bernoulli beam elements which were allowed to have large rotations. To induce buckling numerically we introduced an infinitesimally small imperfection in the membrane, in the form of an initial curvature $\kappa^* = 10^{-4}$ ($\kappa^* = \kappa L_{\mathrm{m}}$ where κ is the curvature of the membrane and L_{m} is the length of the membrane). Buckling of the membrane was produced by clamping one end while imposing a clamped-longitudinal compressive displacement $\delta_L{}^* = \delta_L/L_{\mathrm{m}}$ onto the other end (figure 2(a)). More details on the DEM formulation we used can be found in [16]. This nonlinear system was solved using the iterative Newton–Raphson method [16, 29]. We first present results from the DEM modeling of a plain membrane (free of scales), which we used for validation. The DEM buckling

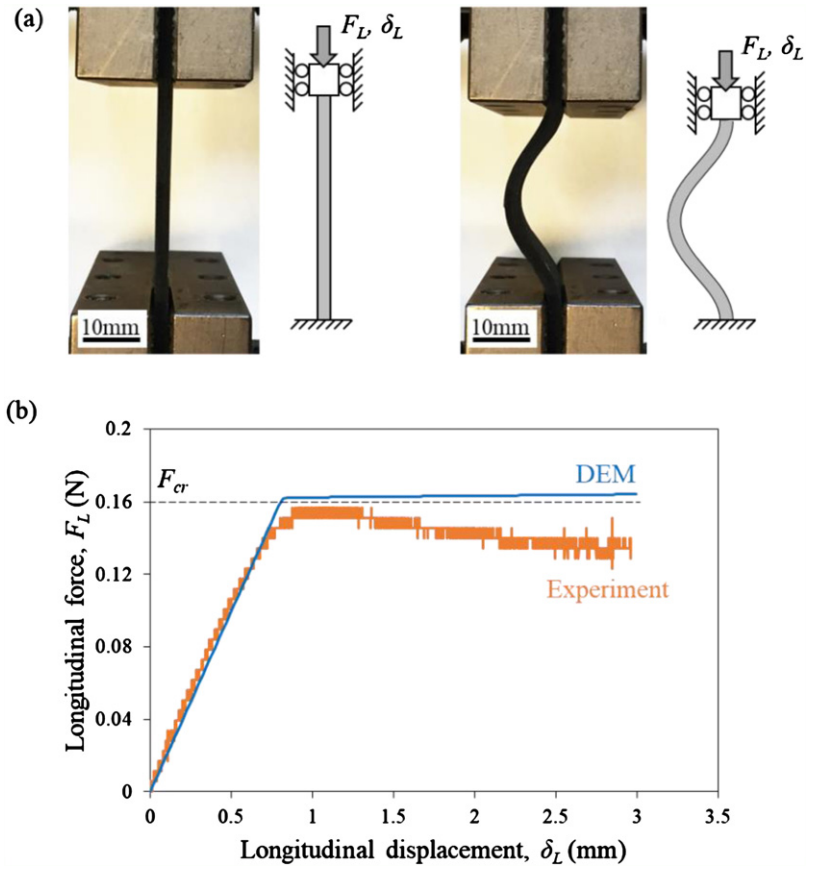

Figure 2. (a) Snapshots and schematics of a buckling experiment on a bare polyurethane membrane with fixed-ends conditions (no rotation); (b) corresponding longitudinal force—longitudinal displacement curves.

model was compared with buckling experiments on a strip of polyurethane (Young's modulus = 4.5 MPa, measured in three-point bending) with a length L_m = 50 mm, thickness t_m = 1.4 mm thick and a width w_m = 10 mm. These buckling experiments were conducted in displacement controlled mode on a dual column universal testing machine (ADMET, model eXpert 5000, MA US) which continuously recorded the axial force F_L as δ_L was increased at a quasi-static rate. Figure 2 shows two representative snapshots of these experiments and a representative F_L–δ_L curve.

As expected, the initial response is linear up to a critical force F_{cr} which marks the onset of buckling. Beyond the point the increasing stresses in the membranes are offset by the geometric softening of buckling, so that the force is decreasing with displacement. The DEM model of the bare membrane is in very good agreement with the experiments in terms of initial stiffness and critical force at buckling. The forces in the buckling region are lower than in the DEM model which we attributed to imperfections in the membrane [33]. We also compared these results with Euler's theoretical critical load of a beam with identical end conditions given by [34]:

$$F_{cr} = \frac{4\pi^2 EI}{L_m^2}. \quad (1)$$

Using the experimental parameters we computed a theoretical critical force F_{cr} = 0.162 (N) which is also in agreement with the DEM model and buckling experiments (figure 2(b)). The next step was to develop DEM models with hard scales perfectly bonded onto the membrane (figure 3(a)). We placed N_s identical scales with normalized length L/L_m and normalized thickness t/L_m on the elastic membrane. The scales were uniformly spaced with a normalized gap distance d/L_m. These geometrical parameters are therefore related by the equation $L/L_m = (1+ (N_s + 1)d/L_m)/N_s$. The thickness of the membrane was on the same order as the thickness of the scales or thinner, and therefore we assumed that the segments of the membrane which were bonded to the scales were perfectly rigid. Only the sections of the membrane which were 'free-standing' between the scales were allowed to deform. In the model, the scales could also interact by direct contact. Scale-to-scale collisions were detected using a shape intersection algorithm (Sutherland–Hodgman polygon clipping [35]) which detected whether a vertex entered the contour of the scale. When a scale-to-scale collision was detected we first established whether interaction occurred by 'sharp contact' where a corner of a scale penetrates a flat edge of another scale, or by 'flat contact' where the neighboring edges from contacting scales interpenetrate and make a four-sided-shape

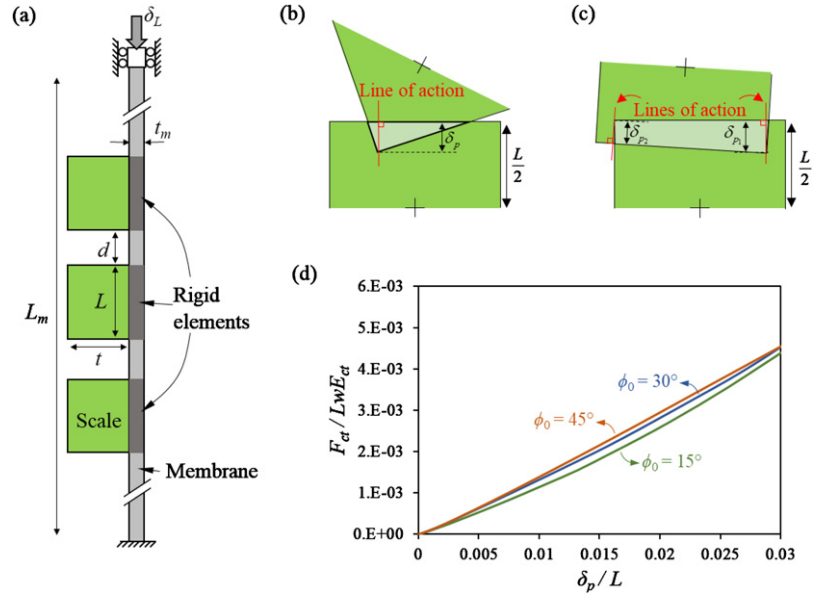

Figure 3. (a) DEM model of a system of hard scales bonded onto a soft membrane with fixed-ends conditions; Schematic showing the penetration of two scales for the case of (b) a 'sharp' contact and (c) a 'flat' contact. For both cases the lines of action of the contact forces are shown in red; (d) The normalized resultant contact as a function of the normalized penetration for the models with different incidence angles, which was used to obtain the constants C_1 and C_2.

overlap (in this case, the shape intersection algorithm detects two penetrating corners). For the case of a sharp contact the penetration distance δ_p was determined as defined on figure 3(b). δ_p was then used to compute the contact force using a model inspired by a Winkler elastic foundation [16, 36]. Assuming that the scales are frictionless the contact force F_{ct} for a 'sharp' contact is written:

$$\frac{F_{\mathrm{ct}}}{LwE_{\mathrm{ct}}} = C_1\left(\frac{\delta_p}{L}\right)^{C_2}, \qquad (2)$$

where E_{ct} is the contact modulus, and w is the out-of-plane width of the scales. The interpenetration of the scales was a streamlined was a streamlined approach to capturing the localized deformation of the scales due to contact forces. To calibrate C_1 and C_2 we used a 2D finite element model of a sharp contact between two identical square scales (ANSYS, V16 2016, PA, US) where one of the scales was rotated by $\phi_0 = 45°$ (incidence angle) from the other one. In this model one scale penetrates the other under controlled displacement [16], and the normalized resultant contact force F_{ct}/LwE_{ct} was computed as a function of the normalized penetration δ_p/L (figure 3(d)). These results were then fitted with equation (2) to determine the constants in model (2): $C_1 = 1.1$ and $C_2 = 0.23$. We repeated the test with different angles of incidence for the penetrating scale (figure 3(d)) and obtained almost identical values for C_1 and C_2. An important ingredient in the scale-scale contact model is the line of action of the contact force F_{ct}, because it governs the moment generated by F_{ct} on individual scales, which in turn govern their rotation. Our definition of the line of action for a 'sharp' contact is shown on figure 3(b): the line of action was defined as a line perpendicular to the edge of the flat contact and intersecting the tip of the sharp contacting scale. The other contact configuration of interest is the 'flat' contact, where the domain of intersection between the scales is four-sided (figure 3(c)). For this case we simply applied equation (2) twice to compute two contact forces (and two distinct lines of actions) generated by the normal penetration δ_{p1} and δ_{p2}.

For validation, we compared a full DEM model of the scaled membrane (including contacts) with experiments. Buckling experiments were performed on a strip of polyurethane covered with scales. The scale dimensions were $t = 2.5$ mm, $L = 7.75$ mm, $w = 10$ mm and were 3D printed with a high resolution direct light projector 3D printer (EnvisionTech Micro HiRes) which produced fully dense, isotropic and pore-free scales with a Young's modulus of 3 GPa (measured experimentally [16]). The scales were then glued onto the surface of the membrane using cyanoacrylate and with a gap distance of $d = 0.5$ mm. The scaled membrane was placed into a loading machine and buckled following the same protocol as for the bare membrane. Since the scales were only attached to one side of the membrane, the system was not symmetric and there were two asymmetric mode I buckling. Following a terminology we previously used to characterize the flexural response of scaled membrane [11], we defined the 'mode I-extrados' buckling as the buckling configuration where the scales, placed on the 'extrados' side of the bent membrane, move apart as bending deformations increase (figure 4(a)). We defined the 'mode I-intrados' buckling as the

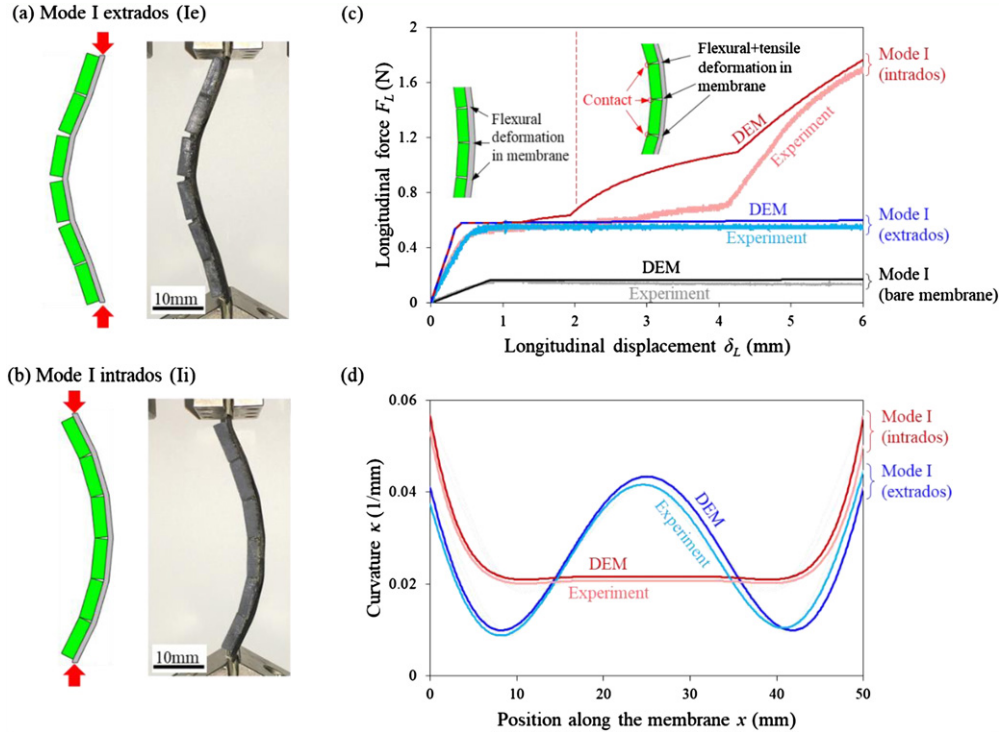

Figure 4. Experimental and DEM buckling test on a scaled polyurethene strip where the system buckles into (a) mode I-extrados and (b) mode I-intrados; (c) longitudinal force-longitudinal displacement curves showing a good agreement between the experimental and DEM results; (d) Curvature of the membrane as a function of the position along the membrane in the mode I-extrados and mode I-intrados configurations at loading point $\delta_L = 6$ mm.

buckling configuration where the scales, placed on the 'intrados' side of the bent membrane, move closer together and may enter contact as bending increases (figure 4(b)). To steer the experiments into either of the mode I-extrados or -intrados, we imposed a small pre-curvature ($\kappa \approx 0.0005$) to the system. Figure 4(c) shows the experimental F_L–δ_L curves for mode I-intrados and mode I-extrados buckling modes, together with the results from the bare membrane for comparison. As expected the scales made the membrane significantly stiffer, which also increased the critical buckling force by a factor of ~3. The effect of the scales on the initial stiffness and critical force was identical for the two buckling modes, and the two buckling responses were identical until the scales entered contact. For the mode I-extrados, the scales moved away from one another and the deformation mechanism was unchanged until the end of the experiment. On the other hand, for the mode I-intrados buckling mode and starting at $\delta_L = 1.2$ mm the scales started to enter contact in the mode I-intrados buckling, which added significant stiffening to the buckling response. We observed a transition regime where the scales progressively entered contact ($1.2 < \delta_L < 4.2$ mm), followed by an extremely stiff regime where all scales where in contact ($\delta_L > 4.2$ mm). In this particular regime, a large contact force is generated between the scales, balanced by a large tension in the membrane that predominantly acted as a tensile ligament. This 'jamming' effect is what generates unwanted stiffening on bio-inspired scaled skin, for example at the palm of gloves (figure 1(b), [11]). Another effect of contacting scales in the intrados mode is the redistribution and 'equalization' of flexural deformations. Figures 4(a) and (b) show snapshots of the buckled scaled membrane well into the stiffening regime ($\delta_L = 6$ mm). Mode I-extrados shows flexural deformations which are localized at the ends and at the middle of the membrane. In contrast, the membrane in mode I-intrados shows more distributed flexural deformations, so most of the membrane forms an almost perfect arc of circle. This effect is better seen by plotting the local curvature of the membrane as function of position (figure 4(d)), showing a near-uniform curvature along most of the membrane. The scales can therefore be used not only to stiffen the membrane and to increase the buckling critical force, but also to control the buckled geometry (in the next section we also explore how the scales can be used to manipulate the stability of the system).

Finally, figure 4 also shows that DEM predictions are in excellent agreement with the experiments, except in the mode I-intrados stiffening where the DEM model overestimates the force (but the onsets of the transitions are captured accurately). We attributed this discrepancy with imperfections in the geometry of the 3D printed scales (imperfect, rounded corners) and their spacing. Nevertheless, the level of accuracy of the DEM model was deemed sufficient to

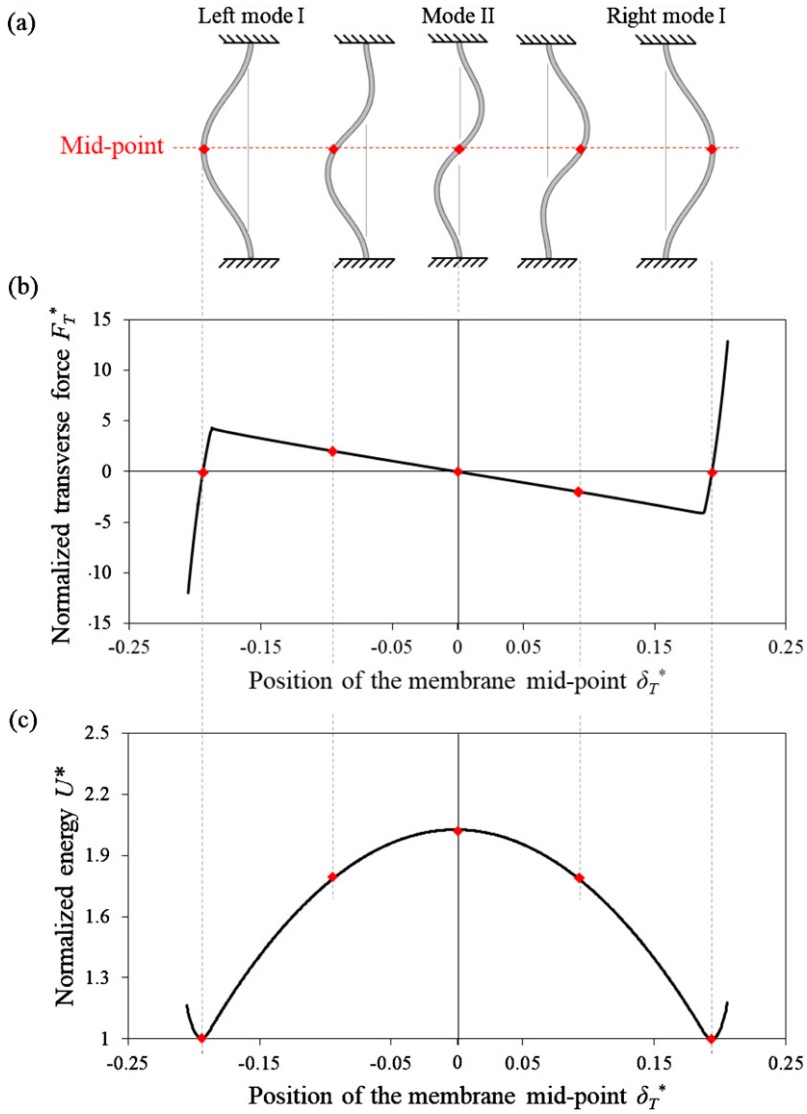

Figure 5. Buckling results from DEM on a bare membrane: (a) Buckling profiles, (b) force landscape and (c) strain energy landscape. To generate this plot a transverse displacement is applied to the mid-point of the membrane.

use it as exploratory tool for the design of the scaled membranes, focusing on the post-buckling regimes.

3. Post-buckling response

Mode I buckling is the only stable mode for a simple and uniform column or membrane in compression. Higher buckling modes exist in theory, but they are not seen in practice because they are unstable. In this study we hypothesised that the scales can be used to manipulate the stability of higher order modes. In particular, we were interested in promoting mode II buckling, which can create wrinkles in natural scaled skin as seen in snake and lizard skins (figure 1). We first started by investigating the stability of a bare membrane in buckling. A buckled system tends to stay in a configuration with the lowest strain energy, therefore, the mode shapes which have a local minimum energy are stable [34]. A possible approach to assess stability is to disturb the buckled configuration with a transverse load and to examine the change in energy and force, and whether these changes induce the system to return to the stable configuration when the disturbance is removed. Here we used the DEM models to apply a transverse displacement to the buckled membrane, while monitoring total strain energy. Figure 5(a) shows a membrane subjected to a normalized longitudinal displacement of $\delta_L{}^* = \delta_L/L_m = 0.1$ and buckled in mode I (We kept the longitudinal displacement $\delta_L{}^* = 0.1$ constant for this numerical experiment). Initially the transverse defection of the midpoint is $\delta_T{}^* = -0.19$ and the force $F_T{}^*$ is equal to zero (figure 5(b)), and the system is in a stable equilibrium which occupies a state of minimum energy. We then imposed a transverse displacement to the mid-point of the membrane to steer the system away from that first stable equilibrium position. Figures 5(b) and (c) show the corresponding transverse force $F_T{}^*$ applied at the mid-point (normalized by $F_T{}^* = F_T L_m{}^2/EI$), and the strain energy of the

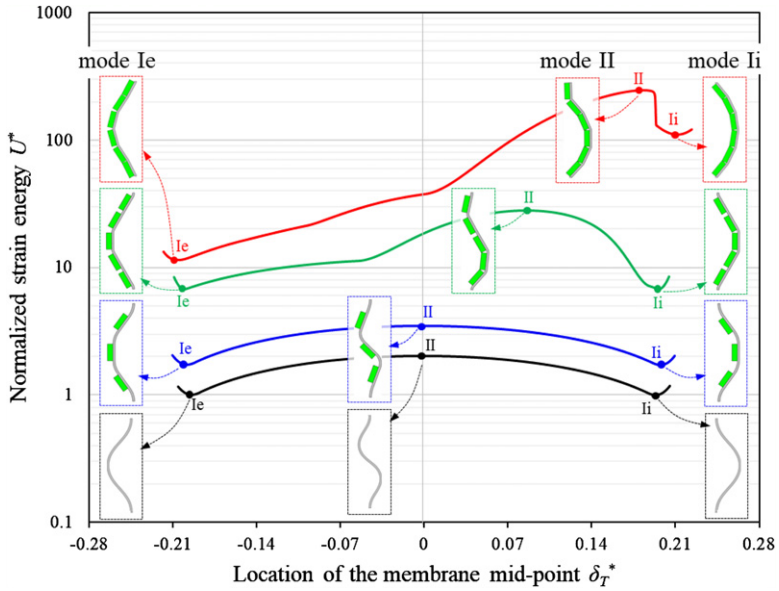

Figure 6. Buckling energy landscape for a bare membrane and a membrane uniformly covered by three, five and six scales with fixed sizes of $t/L_m = 0.05$ and $L/L_m = 0.15$.

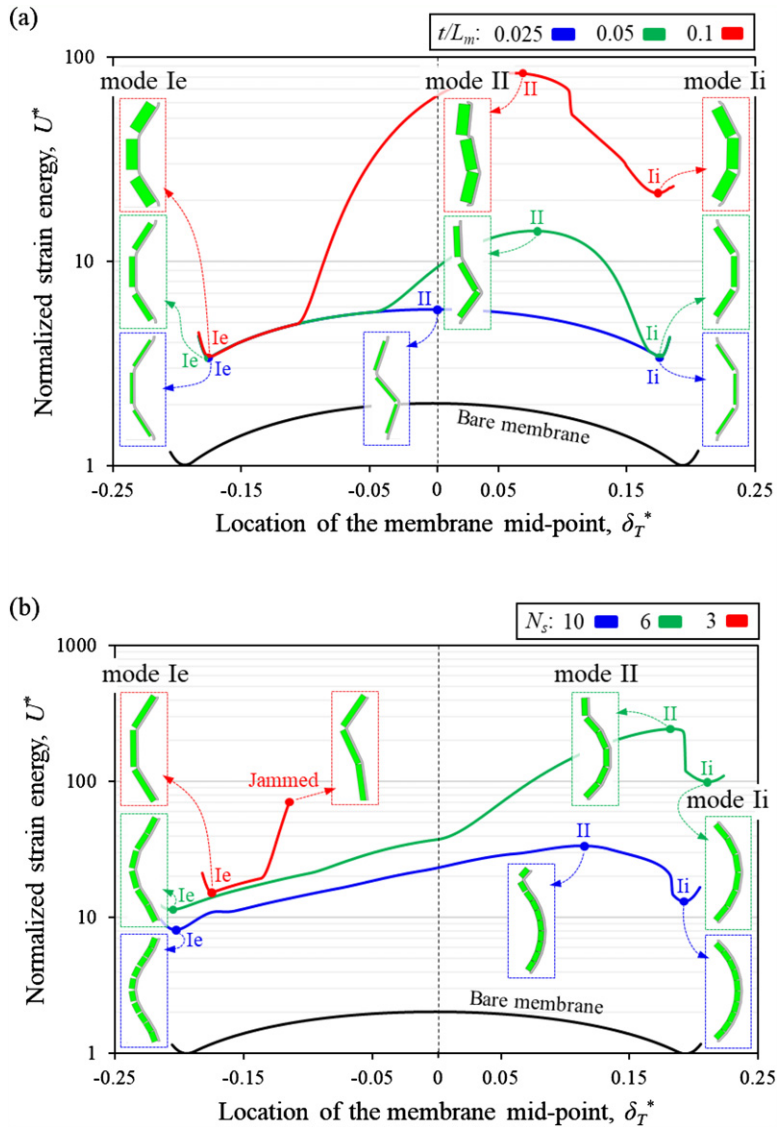

Figure 7. Buckling energy landscape for three different scaled membranes: (a) varying scale thickness with a fixed gap distance of $d/L_m = 0.05$ and scale number of $N_s = 3$; (b) varying number (and length) of the scales for a fixed gap distance of $d/L_m = 0.01$ and scale thickness of $t/L_m = 0.05$. The energy of the bare membrane is also shown for comparison.

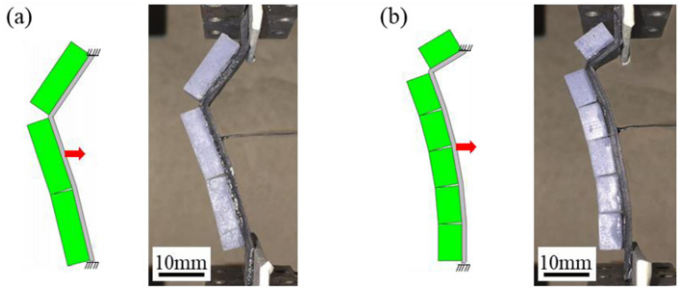

Figure 8. DEM and experimental results on scaled membranes in jammed configurations: with (a) $t/L_m = 0.1$, $N_s = 3$, $d/L_m = 0.01$ and (b) $t/L_m = 0.1$, $N_s = 6$, $d/L_m = 0.01$.

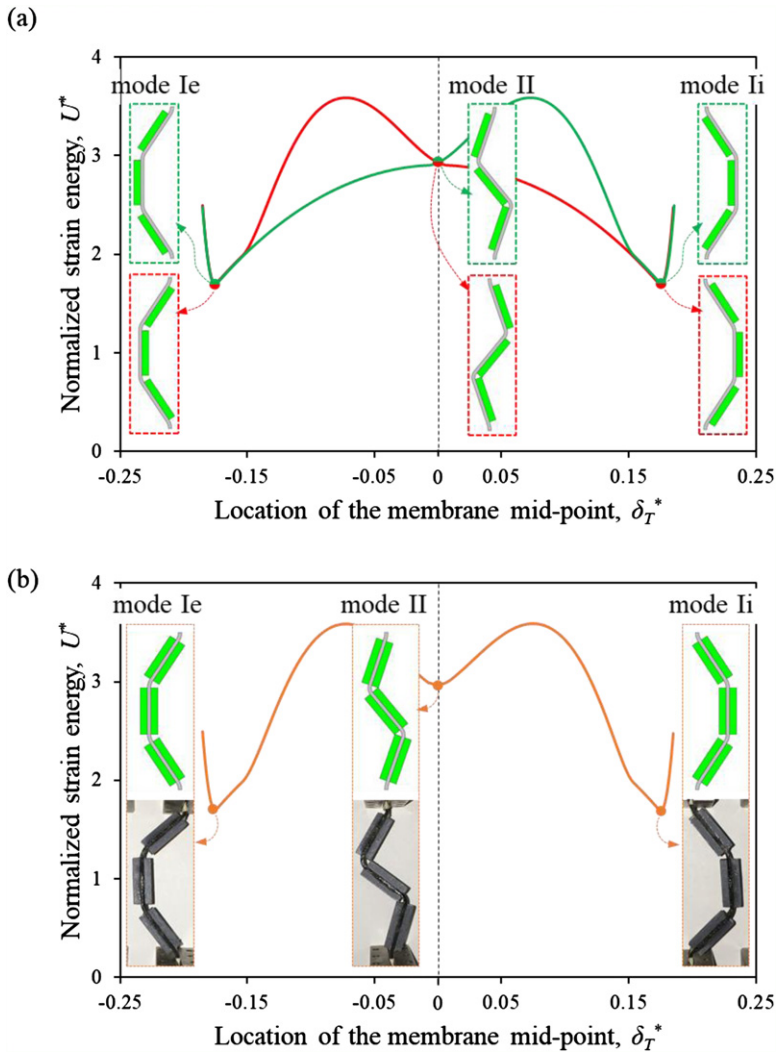

Figure 9. (a) Buckling energy landscape for two models symmetric from one another; (b) the two designs are combined to create a stable mode II.

membrane U^* (normalized by $U^* = U/U_0$ where U_0 is equal to the strain energy of the bare membrane in the mode I) during the transverse displacement, respectively. As the midpoint of the membrane is displaced to the right, $F_T{}^*$ increases, and the system then undergoes a bifurcation at point $\delta_T{}^* = -0.18$ to transition from a 'C" shape to a 'S" shape deformation profile. Following this transition $F_T{}^*$ decreases as $\delta_T{}^*$ is increased further, to reach $F_T{}^* = 0$ at $\delta_T{}^* = 0$.

This state of the membrane corresponds to mode I buckling, another equilibrium solution, which is unstable. Increasing δ_T from that point takes the system to the symmetric mode I buckling configuration, following an antisymmetric $F_T{}^*$–$\delta_T{}^*$ response and a symmetric U^*–$\delta_T{}^*$ response. This simple approach therefore captures the main buckling characteristics of a bare membrane: by two symmetric and stable mode I buckling modes, and one unstable mode II

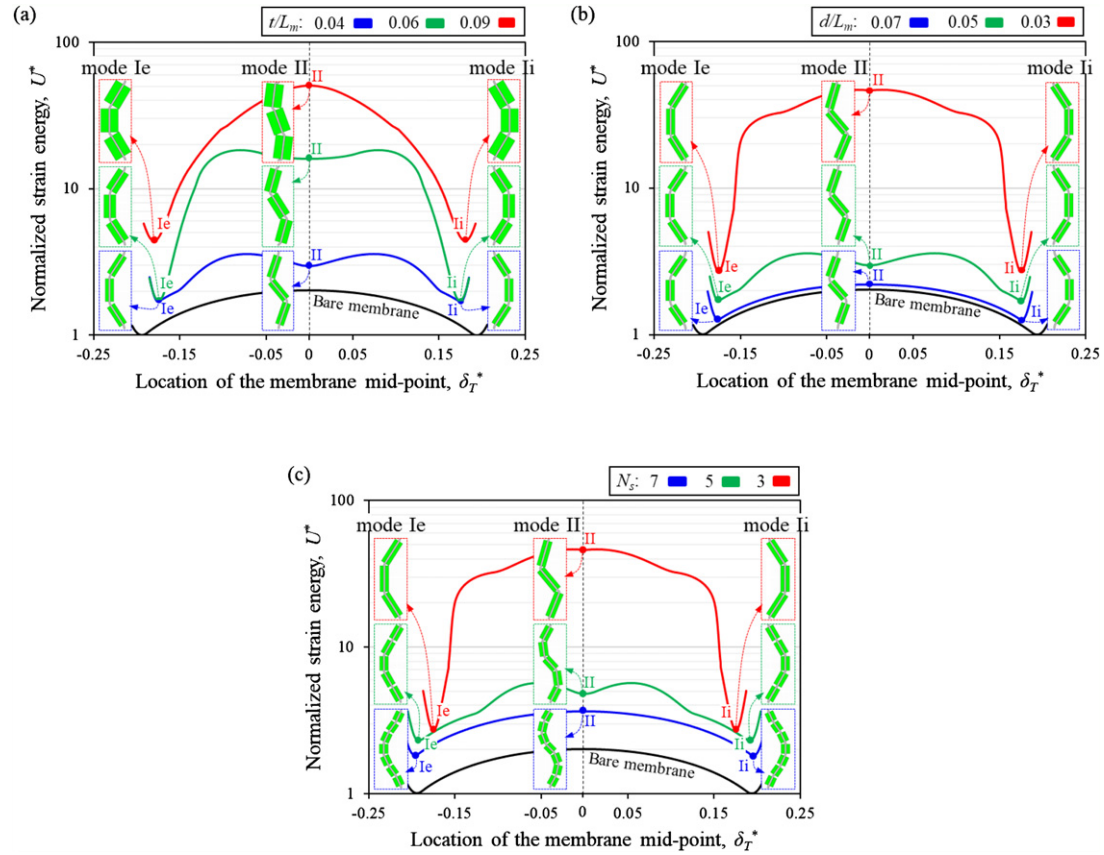

Figure 10. Buckling energy landscape for membranes covered with scales on both sides: (a) varying scale thickness for fixed gap distance of $d/L_m = 0.05$ and scale number of $N_s = 3$; (b) varying scale spacing for fixed scale thickness of $t/L_m = 0.04$ and scale number of $N_s = 3$; (c) varying number (and therefore length) of scales for fixed gap distance of $d/L_m = 0.03$ and scale thickness of $t/L_m = 0.04$.

buckling mode. In the next step, we investigated the effect of the scales in the post-buckling behavior of the system. Figure 6 shows how scales bonded on the membrane (in this example the size of the scales was $t/L_m = 0.05$ and $L/L_m = 0.15$) can drastically change the energy landscape of buckling (if the scales are close enough). If the scales are far apart (blue line in figure 6) no contact is made during buckling, and the only effect of the scales is stiffening (i.e. higher strain energy in the system). If the scales are close enough (green and red lines in figure 6), the scales enter contact during buckling in mode I-intrados, which greatly increases the strain energy and changes the shapes in the energy curve, with a significant rise in energy on the intrados side (right side on the graph). As a result, the mode II positions are shifted to the right (but they remain unstable). We also note that the mode Ii becomes a higher energy mode compared to Ie, and that Ie is more stable (i.e. the energy barriers around Ii are steeper than around Ie). Reducing the gap between the scales (which adds more scales on the membrane) accentuates these effects.

These effects and asymmetries can also be amplified further with thicker scales and larger numbers of (shorter) scales, as shown on figure 7.

Figure 7(b) also shows an extreme configuration where the system is completely jammed around the mode Ie buckling configuration. In this design the scales generate so much locking with such high energy barriers that is it not possible to evolve the system toward mode II and mode Ie buckling. We also captured this phenomenon in experiments where two different models were loaded transversely about a jammed configuration using a wire where one end was glued to the middle of the membrane and the other end was pulled horizontally to the right (figure 8). In these experiments, the only buckling mode that could be achieved was mode Ie. Increasing the transverse force instead resulted in the delamination of the scales from the membrane or failure in the membrane itself. This type of design can be used to only trigger and promote mode Ie, while forbidding the other buckling modes entirely.

4. Buckling of symmetrically scaled membranes

The results above are representative of a large parametric study on scale size and spacing, and while these parameters can change the buckling energy landscape significantly, we did not identify any design

that could increase the stability of mode II buckling. Additional design explorations however revealed that bonding scales on both sides of the membrane could be a powerful approach to stabilizing mode II. Figure 9(a) shows the energy landscape for membranes with scales ($t/L_m = 0.04$ and $d/L_m = 0.05$) bonded to either the left or the right surface of the membrane. As expected, the energy results are asymmetric and both produce higher energy on the intrados side and an unstable mode II buckling mode. Figure 9(b) shows the results of 'superimposing' these two designs by bonding the same scales to both left and the right surfaces of the membrane. This symmetric design takes advantage of the stiffening mechanism associated with contacting scales in both buckling directions, and creates a symmetric energy landscape. The most interesting feature of this design is the emergence of a mode II buckling which is stable, while also preserving the stability of the two modes I. We could validate this result experimentally, creating a scaled membrane with a stable mode II buckling mode (figure 9(b)).

In these symmetric designs, the geometrical parameters (t/L_m, d/L_m, N_s) can be adjusted to increase or decrease the stability of mode II. For example, increasing the thickness of the scale increases the stability of mode II buckling but only up to $t/L_m = 0.06$. Increasing the thickness to $t/L_m = 0.09$ made the maximum strain energy shift to $\delta_T{}^* = 0$ and, as a result, makes the mode II an unstable configuration. Figures 10(b) and (c) show how the spacing of the scales and the number of scales can be tuned to create a stable model II buckling.

5. Summary

A variety of bio-inspired scaled protective systems with useful combinations of flexibility and protection have recently been developed. However synthetic scaled skins stiffen in mode I intrados bending, which reduces the flexibility and dexterity or protective elements like gloves. Nature on the other hand displays examples of scaled skins that can buckle and form wrinkles to accommodate large deformations, a phenomenon which requires higher buckling modes. Inspired from these observations, we explored how rigid scales on a soft membrane impact the energetics of buckling and stability. The main conclusions are as follows:

- Scales increase the strain energy stored in the system by stiffening the membrane and by making direct contact.
- If the scales (bonded on one side of the membrane) are close enough to go in contact in the mode I-intrados, this mode creates a higher energy, and mode I-extrados becomes a more stable configuration.
- 'Jamming' was observed in some designs. This phenomenon can be used to achieve particular buckling modes while excluding others.
- By adding scales onto both faces of a membrane and creating symmetric design, we could create and manipulate a stable buckling mode II.

Greater control of buckling in bio-inspired scaled membrane should lead to better designs of synthetic scale-covered systems. This study provides a strong basis for future designs that guide scaled membrane into specific buckling mode configurations by judicious design and arrangement of rigid protective scales. In particular, the creation of stable mode II buckling configurations can induce wrinkles and folds which can increase the overall flexural compliance and agility of bioinspired protective elements. A prime application of these mechanisms is therefore flexible protection, but there could be other applications in foldable structures or metamaterials where high control and programmability over buckling is desirable. The models we presented here (DEM and 3D printed) are highly idealized and relatively far from natural scaled skin. There are however many obstacles to overcome before a comparison between our model and natural scaled skin can be successful: non-linearities and anisotropies in biological tissues, effect of hydration, rate effects, and last for not least 3D effects. The current model presented here is simplified, but it can nevertheless guide the design of synthetic scales. In addition the design space for scaled skin is vast, and in this study we only focused on 2D rectangular scales. Scales with slanted sides and which overlap, or 3D scales with more complex geometries are known to have a profound impacts on scale-scale interactions and on overall mechanical properties [2–4, 37]. It is also highly probable that buckling is also affect by these additional geometrical features. Further work is needed to examine how enriching the geometry of the scales can be used to access additional buckling modes. These designs may also include non-uniform scales to generate localized deformation mechanisms or to adapt to specific combinations of deformation and constraints [38]. In addition, in this study we only considered perfectly bonded scales and smooth and continuous membranes in this study. In the future, designing and dispersing imperfections in the membrane or incorporating partially debonded scales could be combined to the design of scales for additional tunability of material response [39].

Acknowledgments

This work was supported by a Discovery Grant from the Natural Sciences and Engineering Research Council of Canada. AS was partially supported by a McGill Engineering Doctoral Award.

Data availability statement

The data that support the findings of this study are available upon reasonable request from the authors.

ORCID iDs

Francois Barthelat https://orcid.org/0000-0001-8393-3612

References

[1] Barthelat F 2015 Architectured materials in engineering and biology: fabrication, structure, mechanics and performance *Int. Mater. Rev.* **60** 413–30

[2] Martini R, Balit Y and Barthelat F 2017 A comparative study of bio-inspired protective scales using 3D printing and mechanical testing *Acta Biomater.* **55** 360–72

[3] Yang W, Chen I H, Gludovatz B, Zimmermann E A, Ritchie R O and Meyers M A 2013 Natural flexible dermal armor *Adv. Mater.* **25** 31–48

[4] Vernerey F J and Barthelat F 2010 On the mechanics of fishscale structures *Int. J. Solids Struct.* **47** 2268–75

[5] Mirkhalaf M, Zhou T and Barthelat F 2018 Simultaneous improvements of strength and toughness in topologically interlocked ceramics *Proc. Natl Acad. Sci. USA* **115** 9128–33

[6] Ghods S, Murcia S, Ossa E A and Arola D 2019 Designed for resistance to puncture: the dynamic response of fish scales *J. Mech. Behavior Biomed. Mater.* **90** 451–9

[7] Zhu D, Ortega C F, Motamedi R, Szewciw L, Vernerey F and Barthelat F 2012 Structure and mechanical performance of a 'modern' fish scale *Adv. Eng. Mater.* **14** B185–94

[8] Garrano A M C, La Rosa G, Zhang D, Niu L N, Tay F R, Majd H and Arola D 2012 On the mechanical behavior of scales from Cyprinus carpio *J. Mech. Behavior Biomed. Mater.* **7** 17–29

[9] Meyers M A, Lin Y S, Olevsky E A and Chen P-Y 2012 Battle in the amazon: Arapaima versus piranha *Adv. Eng. Mater.* **14** B279–88

[10] Funk N, Vera M, Szewciw L J, Barthelat F, Stoykovich M P and Vernerey F J 2015 Bioinspired fabrication and characterization of a synthetic fish skin for the protection of soft materials *ACS Appl. Mater. Interfaces* **7** 5972–83

[11] Martini R and Barthelat F 2016 Stretch-and-release fabrication, testing and optimization of a flexible ceramic armor inspired from fish scales *Bioinspir. Biomim.* **11** 066001

[12] Porter M M, Ravikumar N, Barthelat F and Martini R 2017 3D-printing and mechanics of bio-inspired articulated and multi-material structures *J. Mech. Behavior Biomed. Mater.* **73** 114–26

[13] Martini R and Barthelat F 2016 Stability of hard plates on soft substrates and application to the design of bioinspired segmented armor *J. Mech. Phys. Solids* **92** 195–209

[14] Chintapalli R K, Mirkhalaf M, Dastjerdi A K and Barthelat F 2014 Fabrication, testing and modeling of a new flexible armor inspired from natural fish scales and osteoderms *Bioinspir. Biomim.* **9** 036005

[15] Vernerey F J and Barthelat F 2014 Skin and scales of teleost fish: simple structure but high performance and multiple functions *J. Mech. Phys. Solids* **68** 66–76

[16] Shafiei A, Pro J W, Martini R and Barthelat F 2020 The very hard and the very soft: modeling bio-inspired scaled skins using the discrete element method *J. Mech. Phys. Solids* **146** 104176

[17] Rudykh S, Ortiz C and Boyce M C 2015 Flexibility and protection by design: imbricated hybrid microstructures of bio-inspired armor *Soft Matter* **11** 2547–54

[18] Rudykh S and Boyce M C 2014 Analysis of elasmoid fish imbricated layered scale-tissue systems and their bio-inspired analogues at finite strains and bending *IMA J. Appl. Math.* **79** 830–47

[19] Tatari M, Kamrava S, Ghosh R, Nayeb-Hashemi H and Vaziri A 2020 Bending behavior of biomimetic scale covered beam with tunable stiffness scales *Sci. Rep.* **10** 8

[20] Yang W, Chen I H, McKittrick J and Meyers M A 2012 Flexible dermal armor in nature *JOM* **64** 475–85

[21] Ali H, Ebrahimi H and Ghosh R 2019 Bending of biomimetic scale covered beams under discrete non-periodic engagement *Int. J. Solids Struct.* **166** 22–31

[22] Ghosh R, Ebrahimi H and Vaziri A 2014 Contact kinematics of biomimetic scales *Appl. Phys. Lett.* **105** 233701

[23] Ghosh R, Ebrahimi H and Vaziri A 2017 Non-ideal effects in bending response of soft substrates covered with biomimetic scales *J. Mech. Behavior Biomed. Mater.* **72** 1–5

[24] Wang Q and Zhao X 2016 Beyond wrinkles: multimodal surface instabilities for multifunctional patterning *MRS Bull.* **41** 115–22

[25] Warby W 2008 Emerald tree boa snake https://flickr.com/photos/wwarby/ Accessed 11 May 2020

[26] Cogger H 2017 *Christmas Island Chained Gecko Christmas Island Chained Gecko* https://www.iucnredlist.org/species/11559/83321765

[27] Cundall P A and Strack O D L 1979 A discrete numerical model for granular assemblies *Géotechnique* **29** 47–65

[28] Abid N, Pro J W and Barthelat F 2019 Fracture mechanics of nacre-like materials using discrete-element models: effects of microstructure, interfaces and randomness *J. Mech. Phys. Solids* **124** 350–65

[29] Abid N, Mirkhalaf M and Barthelat F 2018 Discrete-element modeling of nacre-like materials: effects of random microstructures on strain localization and mechanical performance *J. Mech. Phys. Solids* **112** 385–402

[30] Pro J W and Barthelat F 2019 Discrete element models of tooth enamel, a complex three-dimensional biological composite *Acta Biomater.* **94** 536–52

[31] Pro J W and Barthelat F 2020 Discrete element models of fracture in tooth enamel: failure mode competition and statistical effects *J. Mech. Phys. Solids* **137** 103868

[32] Pro J W and Barthelat F 2020 Is the Bouligand architecture tougher than regular cross-ply laminates? A discrete element method study *Extreme Mech. Lett.* **41** 101042

[33] Case J, Chilver L and Ross C T F 1999 Buckling of columns and beams *Strength of Materials and Structures* 4th edn ed J Case, L Chilver and C T F Ross (London: Butterworth-Heinemann) pp 424–57

[34] Timoshenko S and Gere J M 2009 *Theory of Elastic Stability* (New York: Dover)

[35] Sutherland I E and Hodgman G W 1974 Reentrant polygon clipping *Commun. ACM* **17** 32–42

[36] Johnson K L 1987 *Contact Mechanics* (Cambridge: Cambridge University Press)

[37] Varshney S, Song J, Li Y, Boyce M C and Ortiz C 2015 Morphometric structural diversity of a natural armor assembly investigated by 2D continuum strain analysis *J. Struct. Biol.* **192** 487–99

[38] Connors M *et al* 2019 Bioinspired design of flexible armor based on chiton scales *Nat. Commun.* **10** 5413

[39] Budiansky B and Hutchinson J W 1966 *Dynamic Buckling of Imperfection-Sensitive Structures* (Berlin: Springer) pp 636–51